2016

Quantifying Early-Seral Forest Composition with Remote Sensing

Rayma a. Cooley
United States Forest Service

Peter T. Wolter
Iowa State University, ptwolter@iastate.edu

Brian R. Sturtevant
United States Forest Service

Quantifying Early-Seral Forest Composition with Remote Sensing

Rayma A. Cooley, Peter T. Wolter, and Brian R. Sturtevant

Abstract

Spatially explicit modeling of recovering forest structure within two years following wildfire disturbance has not been attempted, yet such knowledge is critical for determining successional pathways. We used remote sensing and field data, along with digital climate and terrain data, to model and map early-seral aspen structure and vegetation species richness following wildfire. Richness was the strongest model (RMSE = 2.47 species, Adj. R^2 = 0.60), followed by aspen stem diameter, basal area (BA), height, density, and percent cover (Adj. R^2 range = 0.22 to 0.53). Effects of pre-fire aspen BA and fire severity on post-fire aspen structure and richness were analyzed. Post-fire recovery attributes were not significantly related to fire severity, while all but percent cover and richness were sensitive to pre-fire aspen BA (Adj. R^2 range = 0.12 to 0.33, p <0.001). This remote mapping capability will enable improved prediction of future forest composition and structure, and associated carbon stocks.

Introduction

Individual wildfires often include a range of impacts (i.e., severity), producing a mosaic of biological legacies that can have persistent influence on post-fire composition and successional pathways (Franklin *et al.*, 2007). Patterns of early-seral forest composition and density established within a few years post-fire are strong predictors of the initial successional trajectory of a forest (Johnstone *et al.*, 2004). In regions with rich fire legacies, the consequences for future dynamics of subsequent forests are dramatic (Johnstone *et al.*, 2010). For example, in boreal and sub-boreal systems of North America, the relative dominance of conifer versus deciduous tree species will strongly affect nutrient dynamics (Frelich and Reich, 1995), fire behavior (DeByle and Winokur, 1985; Carlson *et al.*, 2011), susceptibility to insect disturbance (Charbonneau *et al.*, 2012), wildlife habitat (Pastor *et al.*, 1988), and regeneration capacity in response to future disturbances (Frelich, 2002). A growing body of literature suggests that anthropogenic activities and effects, including climate change, land use, and fire suppression, are modifying regional patterns in fire severity (Stephens *et al.*, 2014). Yet current understanding of the effects of fire severity on forest development lags behind (Keeley, 2009), in part because early-seral regeneration patterns are difficult to quantify at the scale of large burns. Hence, the ability to accurately characterize early-seral forest structure soon after disturbance is of critical importance for understanding successional trajectories.

Remote sensing has been used in boreal and sub-boreal forests of North America to reliably map mature forest composition and structure (Wolter *et al.,* 2009; Wolter and Townsend, 2011). However, the spectral signal of early-seral forest regeneration (one to two years) following disturbance is often indistinct and may be confused with other vegetation life forms, coarse woody debris, and soil prior to canopy closure, which complicates the composition and structure mapping process using medium spatial resolution sensors such as Landsat (Veraverbeke *et al.,* 2012). Nevertheless, the ability to map tree species recruitment and structure information so early in a forest's successional state (over large landscapes) would be a valuable asset for forest managers and scientists in providing insight into future forest development patterns in time and space (Veraverbeke *et al.,* 2012).

The Pagami Creek Fire (PCF, 18 August to 12 October 2011) burned over 38,000 hectares (ha) of the Superior National Forest (SNF), most of which (90.2 percent) occurred in the Boundary Waters Canoe Area Wilderness (BWCAW) (Figure 1). The PCF is the largest and most recent in a series of major fires affecting the BWCAW. The initial behavior of the fire was characterized by low-intensity surface fires, until mid-September when the fire transitioned to a high-intensity crown-fire, creating a range of fire severity patterns. Prior to the burn, this area served as a hotspot for remote sensing research mapping forest composition and structure (Wolter *et al.,* 2008; Wolter *et al.,* 2009; Wolter and Townsend, 2011). The PCF therefore provided a rare opportunity to investigate interactions between pre-fire forest conditions and fire severity as they affected post-fire regeneration patterns. Among the first tree species to emerge from the fire disturbance were quaking and bigtooth aspen (*Populus tremuloides* and *P. grandidentata*, respectively), which can sprout vigorously from clonal root networks (Frelich and Reich, 1995).

The objectives of our study were twofold. First, we assessed the degree to which early regeneration structure of aspen and vegetation species richness could be reliably estimated and mapped using field-collected data measurements, in conjunction with image-based remote sensing variables and other spatially-explicit biophysical information. To our knowledge, two years post-disturbance is the earliest that detailed mapping of aspen regeneration structure (i.e., height, basal area, stem density, stem diameter, and percent cover) has been attempted using image-based remote sensing techniques. Indeed, two-year aspen regeneration is expected to be short, mixed with both herbaceous and woody growth, with either sparse or heterogeneous leaf area that may be well below the spatial resolution of commonly-used satellite sensors such as Landsat (30-meter) to detect. We therefore integrated Landsat imagery with one meter spatial resolution National Agriculture Imagery Program (NAIP) color-infrared aerial image data to develop image-based models of aspen regeneration abundance and structure, as well as vegetation species richness.

Rayma A. Cooley is with the US Forest Service, Six Rivers National Forest, 741 State Hwy 36, Bridgeville, CA 95526, and formerly with the Iowa State University (raymacooley@fs.fed.us).

Peter T. Wolter is with the Iowa State University, 339 Science Hall II, Ames, IA 50011.

Brian R. Sturtevant is with the US Forest Service, Northern Research Station,5985 Highway K, Rhinelander, WI 54501.

Photogrammetric Engineering & Remote Sensing
Vol. 82, No. 11, November 2016, pp. 853–863.
0099-1112/16/853–863

doi: 10.14358/PERS.82.11.853

The development of empirical models of post-fire aspen abundance, aspen structure, and vegetation species richness maps set the stage for our second objective, i.e., evaluating (a) the degree to which mapped biophysical variables improved upon Landsat and NAIP predictors in modeling early-seral vegetation structure following fire, and (b) the relative consistency between empirical models and hypothesized relationships between biophysical variables and early-seral vegetation response variables. Mapped biophysical variables include pre-fire aspen basal area (Wolter and Townsend, 2011), a fire severity proxy (i.e., relative difference normalized burn ratio, RdNBR; Miller and Thode, 2007), terrain, and climate variables. Prior research (Heinselman, 1996; Johnson *et al.*, 2003) suggests that pre-disturbance forest species composition largely determines post-disturbance forest regeneration, implying that pre-fire aspen abundance (irrespective of fire severity) would strongly correlate with post-fire aspen abundance. On the other hand, given sufficient fire residence time, heat penetration into soil can be damaging to aspen root stocks (Brown and DeByle, 1987; Perala, 1991). Other studies have found that fire severity can enhance subsequent dominance by aspen (Frelich and Reich 1995; Fraser *et al.*, 2004). In the case of the PCF, we hypothesized that higher fire severity areas would positively affect aspen abundance and negatively affect species richness (Turner *et al.*, 1997; Wang and Kemball, 2005). We also hypothesized that areas with higher pre-burn aspen abundance would have higher post-fire species richness, because the presence of aspen is known to mitigate fire severity (DeByle and Winokur, 1985; Carlson *et al.*, 2011), as aspen stands tend to have lower fuel accumulations (DeByle and Winokur, 1985). Finally, environmental variables such as climate (precipitation and temperature) and terrain (elevation, slope, and aspect) affect both soil temperature and moisture, and vegetation response dynamics (Frey *et al.*, 2003).

We applied xPLS regression (Wolter *et al.,* 2012) to identify parsimonious sets of predictors (remote sensing and biophysical) to facilitate model calibration and mapping of respective aspen structural parameters and species richness (Objective 1). We then examined the degree to which biophysical predictor variables influenced modeled vegetation structure results (Objective 2) based upon (a) variable coefficients and component loadings produced by the xPLS models, (b) the relative consequence of dropping individual biophysical variables from xPLS models, and (c) the magnitude of correlations between these biophysical predictor variables and measured aspen and vegetation structure field data.

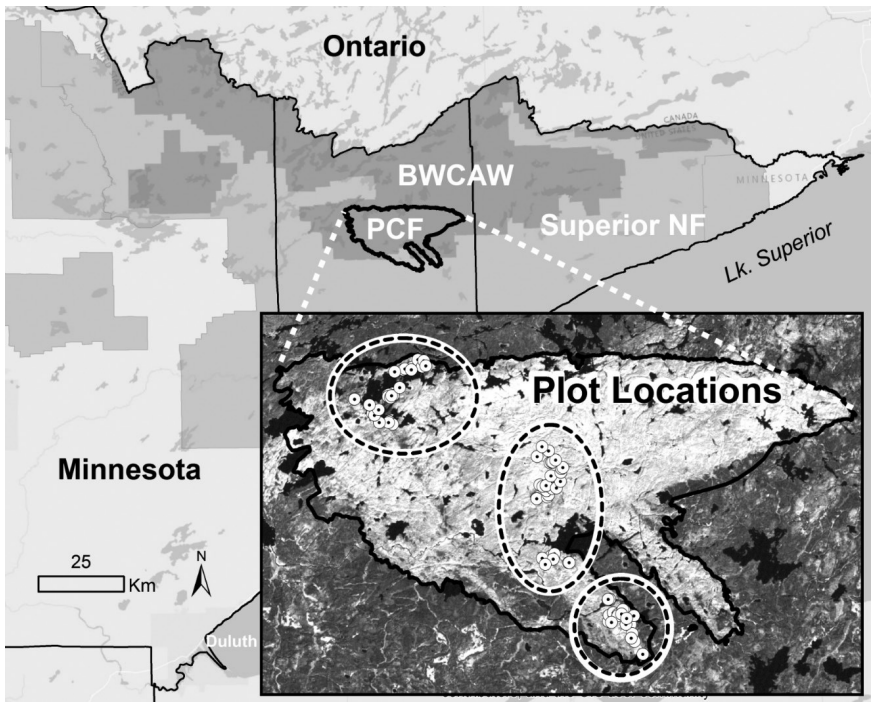

Figure 1. Location of the Pagami Creek Fire (PCF, August to October 2011) and field plot locations within the Boundary Waters Canoe Area Wilderness (BWCAW) of the Superior National Forest in northeast Minnesota.

Methods

Study Area and Field Methods

The BWCAW is located on the southern edge of the North American boreal forest in northeast Minnesota (Figure 1). This landscape lies within the Northern Superior Upland physiographic province and is characterized by numerous lakes, streams, bogs, forested peatlands, and variable soil textures (Heinselman, 1996). The climate is characterized by long cold winters and short warm summers. Mean annual temperature (TEMP) and precipitation (PRECIP) are 3.5°C and 65.0 cm, respectively (NCDC NOAA, 1999-2012). Prevailing winds are from the west (Heinselman, 1996). Lightning-caused wildfires in the region, such as the PCF, are generally associated with clear, dry weather, high temperatures, and rapid fuel drying (Heinselman, 1996; Johnson *et al.*, 2003).

Forest cover types in this region consist of conifer, deciduous, and mixed wood forests. Jack pine (*Pinus banksiana*), black spruce (*Picea mariana*), and balsam fir (*Abies balsamea*) dominate coniferous stands, while quaking aspen and paper birch (*Betula papyrifera*) prevail in deciduous stands (Heinselman, 1996; MN DNR, 2003).

We established 81 field plots within three areas in the PCF (Figure 1) that were within 500 meters of either BWCAW hiking trails or accessible waterbody shorelines. Access to the interior of the BWCAW is difficult due to the roadless wilderness terrain. Within these three broad areas, all plot locations were defined prior to the first field survey using stratified random sampling. Two spatial variables were used for stratification: pre-burn aspen BA (Wolter and Townsend, 2011) and satellite-derived fire severity (RdNBR calculated using pre- [26 June 2009] and post-fire [06/10/2011] Landsat-5 data). These two spatial data layers were also used to assess whether the 81 field plots were representative of the entire PCF, by comparing standard descriptive statistics for the 81 sites to corresponding statistics for the entire PCF.

Vegetation measurements at these plot locations were collected between 27 May and 15 August 2013. We used two separate plot configurations in collecting our data: (a) the relevé method, as developed by the Minnesota Department of Natural Resources (MNDNR, 2013), was used to measure aspen percent cover and vegetation species richness; (b) all other aspen measurements were derived from subplot measurements (Figure 2). Within each plot, four subplots were arranged such that subplot 1 was plot center and subplots 2, 3, and 4 were 18 meters from plot center with 120° spacing (Figure 2). The azimuth from plot center (subplot 1) to subplot 2 was randomly assigned. Subplots were circular with a 3-meter fixed radius (28.27 m^2 area). Combined area of the four subplots, which comprised the full plot area, was 113.10 m^2. The subplot configuration described above was designed to integrate with a range of sensor pixel resolutions (e.g., 2-, 5-, 10-, 20- and

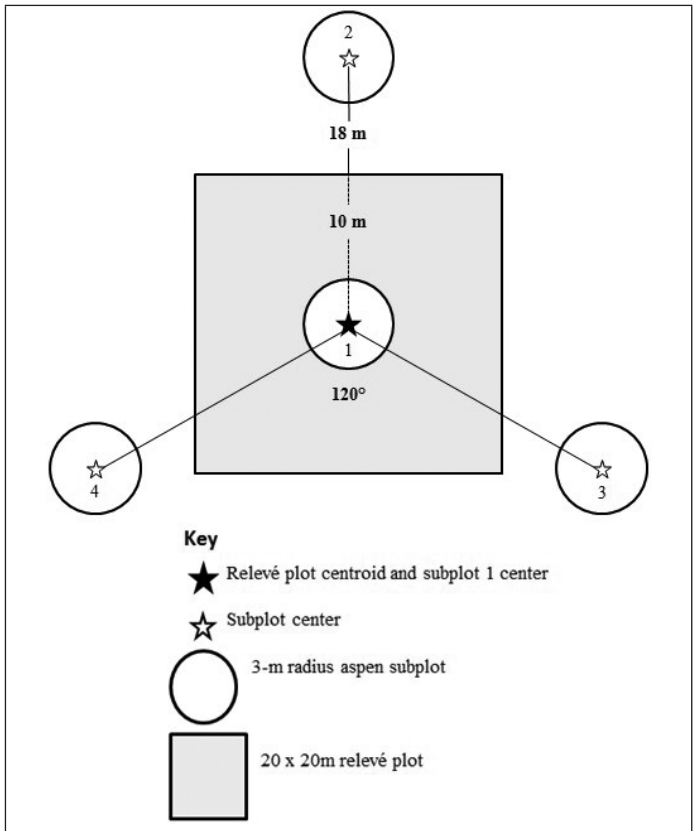

Figure 2. Plot design for relevé and aspen measurements includes a large 20 × 20 m relevé plot and four, 3-m radius; subplots: one at plot center and three, evenly placed, subplots.

30-m). The combined area of the four subplots is 28.3 percent of a 20-m pixel and 12.6 percent of a 30-m pixel. Relevé methodology was developed to describe and classify plant communities (MNDNR, 2013), and was thus more appropriate in measuring aspen percent cover and vegetation species richness. Percent cover of all vascular plant species present within a 20 × 20 meter area were classified into six categories across a range of 0 to 100 percent cover (class 1: <1 percent; class 2: 1 to 5 percent; class 3: 5 to 25 percent; class 4: 25 to 50 percent; class 5: 50 to 75 percent; and class 6: 75 to 100 percent). If percent cover was less than 5 percent, abundance of individual species was further divided into three sub-classes (sub-class 1: single individual; sub-class 2: 2 to 20 individuals; and sub-class 3: many individuals. The relevé plot area (0.04 ha) represents approximately 44.4 percent of a 30-m Landsat pixel.

We collected aspen structure measurements (stem count, diameter, height, and BA) and soil depths to bedrock within each of the four subplots per plot (Figure 2). While all aspen stems were counted, a minimum of 10 stems per subplot were systematically selected for measurement by first counting all stems, dividing the count by 10 (count/10 = n), and then measuring every n^{th} stem for diameter at root collar and height. Soil depth to bedrock was measured by pounding a 1.5-meter steel rod into the ground at plot center and at the center of all subplots, until either refusal at bedrock or maximum depth was reached. Aspen within field plots sampled in May and June of 2013 (n = 32) were re-measured between 19 and 23 May 2014 (while dormant) to account for early season growth, ensuring that measurements corresponded with late season sensor overpass times (Table 1A). In total, we sampled vegetation at 81 plots: 28 in the northwest region of the burn, 22 in the central region, and 31 in the south-central region (Figure 1).

Aspen stem density (DEN), average number of aspen stems per square-meter, was calculated by dividing the total aspen count (TAC) of the pooled subplots by the pooled subplot

Table 1. (A) Remote Sensing Source Imagery and Derived Indices (Predictors) Used with Ground Data (Response Variables) to Calibrate Aspen Structure and Vegetation Richness Models for the Pagami Creek Fire Study Area; (B) Ancillary Digital Variables Used in Addition to Derived Remote Sensing Indices as Predictors for Calibrating Vegetation Structure Models

(A)

Image Data	Image Codes	Date	Pixel (m)	Bands	Raw Bands (μm)	Band Code	Derived Indices
Landsat 8	L8	16/09/2013	30	7	0.435-0.451 0.452-0.512 0.533-0.590 0.636-0.673 0.851-0.879 1.566-1.651 2.107-2.294	CA/1 BL/2 GR/3 RD/4 NIR/5 SWIR1/6 SWIR2/7	SR[1], NDVI[2], MSI[3], NBR[4], RA[5], SVR[6]
Landsat 7	W1	23/01/2014	30	6	0.441-0.514 0.515-0.601 0.631-0.692 0.772-0.898 1.547-1.749 2.064-2.345	BL/1 GR/2 RD/3 NIR/4 SWIR1/5 SWIR2/7	SR, NDVI, MSI, RA, SVR
NAIP[7]	N2, N5, N10, N20, N30	18/09/2013	2, 5, 10, 20, 30	4/res.	blue, green, red, near-IR	BL, GR, RD, NIR	SR, NDVI (per resolution)

(B)

Ancillary Data	Source	Pixel (m)	Layers	Layer Name	Layer Code
Climate	PRISM	4000	4	Annual precip. Mean temp. Min. temp. Max. temp.	PRECIP MEAN_TEMP MIN_TEMP MAX_TEMP
Terrain	SRTM	30	3	Elevation Slope Aspect	ELEV SLP ASP
2011 Aspen BA	Wolter & Townsend (2011)	30	1	Pre-fire aspen BA	PF_ASP_BA

[1] Simple ratio, NIR/red
[2] Normalized difference vegetation index, {[(NIR-red)/(NIR+red)] +1}*100)
[3] Moisture stress index, SWIR1/NIR
[4] Normalized burn ratio, [(NIR-SWIR2)/(NIR+SWIR2)]+1]
[5] Reflectance absorption index, NIR/(red+SWIR1)
[6] Shortwave-IR to visible ratio, ((SWIR1+SWIR2)/(blue+green+red))*1.5
[7] National Agriculture Imagery Program

sample area (113.1 m^2). Aspen stem diameter (DIA; mm) was calculated as the pooled subplot average diameter at root collar. Aspen stem height (HT; cm) was calculated as the average height of stems in the pooled subplots. Average aspen dimensions for each pooled subplot area (i.e., DIA and HT) were estimated using a systematic subsample of stems counted (i.e., every tenth stem). Aspen percent cover (PC) parameter was based on *in situ* ocular estimates of foliar cover according to relevé methodology (MNDNR, 2013). Aspen basal area (BA, mm^2m^{-2}) was computed as DEN multiplied by average stem cross-section area (mm^2) divided by the combined area of the pooled subplots (113.1 m^2). Vegetation richness (RIC) was calculated as the total number of plant species found in each plot's 0.04 ha relevé sample area.

Predictor Variables

Both satellite- and aircraft-based remote sensing image data were used in this research (Table 1A). Two Landsat images from two sensors (Landsat-7 and -8; W1 and L8, respectively) were acquired from USGS Earth Resources Observation and Science Center (EROS, *http://glovis.usgs.gov/*) for the PCF area (WRS-2 path 27, row 27). We included winter Landsat-7 imagery (W1; Table 1A) as a potential predictor of aspen abundance to take advantage of relationships between tree shadows cast on snow-covered ground and quantitative measures of wood volume (Wolter *et al.*, 2012). It should be noted that the 23 January 2014 Landsat-7 winter image (W1) had known scan line corrector (SLC) failure errors, which result in a striped pattern of image data dropouts that radiate out (with increasing width) from the sensor's nadir ground track. A total of 9 ground plots fell within these dropout areas, and were removed from models that retained this variable (described below in *Analyses*). One meter spatial resolution National Agriculture Imagery Program (NAIP) color-infrared aerial image data (flown August 2013) were also acquired (*http://datagateway.nrcs.usda.gov/*). Raw NAIP imagery (1 m) was too fine a resolution for predicting aspen abundance and structure estimated from our plot layout design, due to the spatial heterogeneity of observed aspen abundance. Nonetheless, it was unclear as to which spatial resolution would be optimal. Therefore, we degraded the raw NAIP imagery to 2-, 5-, 10-, 20-, and 30-m resolutions (hereafter referred to as N2, N5, N10, N20, and N30, respectively) in an effort to identify appropriate spatial scales for model development (Table 1A).

We calculated several spectral indices (from imagery described above) as additional predictors of post-fire vegetation structure (Table 1A). These indices are well established in vegetation remote sensing literature and include:

1. vegetation simple ratio (SR; Jordan, 1969),
2. normalized difference vegetation index (NDVI; Rouse *et al.*, 1974),
3. moisture stress index (MSI; Rock *et al.*, 1986),
4. normalized burn ratio (Key and Benson 2005),
5. reflectance absorption index (RA, Arzani and King, 1997), and
6. shortwave infrared to visible ratio (SVR, Wolter *et al.*, 2008).

Shortwave infrared bands and indices (e.g., Landsat-7 bands 5 and 7, MSI, and SVR) were used as these wavelengths and indices are known to be sensitive to forest BA (Wolter *et al.*, 2008) (Table 1A). The normalized burn ratio (NBR, [Band4-Band7] / [Band4+Band7]), introduced by Key and Benson (2005), was used along with the other indices as potential post-fire predictors of aspen and vegetation structure. Later we calculate the relative difference NBR (RdNBR, Miller and Thode, 2007) as our specific proxy for fire severity to better understand factors leading to observed and modeled forest responses following fire. In that capacity, RdNBR is the difference between pre- and post-fire NBR divided by the square root of the absolute value of pre-fire NBR/1000. This formulation is said to reduce sensitivities to species-specific chlorophyll type and density that otherwise bias the NBR and difference NBR (dNBR) formulations (Miller *et al.*, 2009). Correspondence between RdNBR values and ground-based measures of fire severity is known to be ca. 80 percent (R^2) in coniferous systems (Miller *et al.*, 2009). We calculated RdNBR using pre- and post-fire Landsat-5 sensor data (26 June 2009 and 06 October 2011, respectively; each having the highest image quality code) for the entire PCF region to serve as a spatially explicit proxy for fire severity (Plate 1).

Terrain information (elevation, aspect, and slope) was derived from a 30-m digital elevation model (DEM) from the Shuttle Radar Topography Mission (*http://www2.jpl.nasa.gov/srtm/*). Terrain aspect was converted to eight thematic direction classes prior to use in this study. Four kilometer spatial resolution climate data (precipitation and temperature estimates) for the region and time period were acquired from PRISM Climate Group, Oregon State University (*http://prism.oregonstate.edu*). Lastly, mapped estimates of pre-fire aspen BA and distribution, as well as overall species composition, derived by Wolter and Townsend (2011), were acquired from the authors and used in this study (Table 1B). These ca. 2008 data consist of continuous estimates of mature forest BA mapped to 30-meter spatial resolution for eight conifer and four hardwood species (aspen BA precision: R^2 = 0.89; RMSE = 6.64 $m^2 \cdot ha^{-1}$) across the entire PCF region. This initial set of 58 predictor variables was used with xPLS regression (see Wolter *et al.*, 2012) to develop respective models of aspen structure and vegetation (described below in *Analyses*).

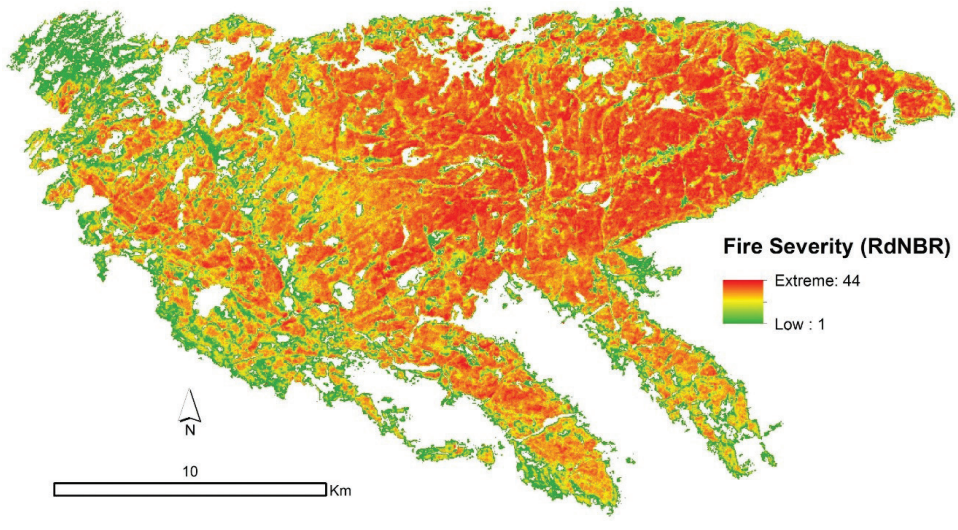

Plate 1. Relative difference normalized burn ratio (RdNBR; Miller et al., 2009) calculated for the PCF using before (26 June 2009) and after burn (06 October 2011) Landsat imagery, from low (green) to extreme (red) fire severity.

Spatially explicit proxies for soil depth did not exist at the time this research was conducted, which precluded use of our soil depth measurements for vegetation structure mapping. Hence, exploratory simple linear regressions of our soil depth measurements on aspen structure and vegetation richness were conducted at the plot-level only.

Analyses

Model calibrations between field estimates of aspen structure (i.e., DIA, HT, PC, BA) and vegetation richness (RIC) variables and image and biophysical predictor variables were accomplished using an iterative form of partial least squares regression (PLS; Geladi and Kowalski, 1986) called iterative exclusion partial least square regression (xPLS, Wolter *et al.*, 2012). Center locations from the 81 field plots were used to extract respective point samples of all predictor variables in these analyses. Our goal in using xPLS was to find the most parsimonious model (i.e,. fewest variables) that would explain the largest amount of variation in the dependent vegetation structure variables. The iterative xPLS regression and variable selection approach is ideal (especially in remote sensing) because the underlying PLS regression routine provides a means to condense a large number of collinear variables down to a few salient, non-correlated, latent structures or components (Wolter *et al.*, 2008). The xPLS approach differs from stepwise and AIC/BIC methods in that xPLS uses leave-one-out cross-validation to (a) choose the appropriate number of components to use at each step, (b) eliminate predictor variables that show no or low response to the dependent variables, and (c) validate resulting final models (Wolter *et al.*, 2008). Issues related to multicollinearity related to the large number of potential predictor variables are minimized but not eliminated using this method (see below).

The final, reduced set of image predictor variables and associated regression coefficients were then used to map vegetation patterns (i.e., aspen abundance, aspen structure, and species richness) to upland areas of the PCF. Wetlands and non-forest areas were neither mapped nor considered in subsequent analyses. We used the US Fish and Wildlife Service's National Wetlands Inventory Program (NWI) data (*https://www.fws.gov/wetlands/index.html*) to mask all wetland areas. Weekly snow depth maps (*http://climate.umn.edu/doc/snowmap.htm*) were used to select Landsat imagery (08 February 2011) with sufficient snow cover (76 to 80 cm) to assist in masking out snow-covered, non-forest areas (see Wolter *et al.*, 2008). We used standard descriptive statistics to evaluate the degree to which biophysical variables for the 81 field plot locations were representative of the mapped and observed ranges of natural variability in these data, respectively, across the mapped PCF area. We mapped the final vegetation structure models across the PCF at 2 m pixel resolution, which was the minimum pixel size (NAIP) among the respective reduced sets of image variables.

We emphasize that xPLS regression iteratively determines the optimal number of latent structures (components) to use for each successive variable set under consideration ($n - 1$) within the iterative xPLS variable selection routine (Wolter *et al.*, 2008; Wolter *et al.*, 2012). While the final set of predictor variables represents the optimal combination to enable effective mapping of the response variables, the regression coefficients linking the final set of correlated predictors to their associated, non-correlated latent structures remain interdependent. Hence, this fact may complicate the degree to which we can reliably use the coefficients themselves (i.e., direction, magnitude) to evaluate specific hypotheses regarding the underlying causal relationships generating the patterns. We therefore explored the role of individual biophysical variables (specifically pre-fire aspen basal area and burn severity) potentially affecting vegetation recovery patterns by systematically dropping these variables and repeating the xPLS procedure, and evaluating the consequences in terms of their significance ($\alpha \leq 0.05$), R^2, RMSE, and the number of variables the alternate models retained. In addition, simple linear regression was used to evaluate the independent strength of correlations between each of the plot-derived values of DEN, DIA, HT, PC, BA, and RIC and both fire severity and pre-fire aspen BA predictor variables.

Results

Plot Data

Two years post-fire, the average aspen cover recorded within the relevé plots was just under 10 percent, and ranged between 0 and 88 percent. Pooled subplot-level aspen regeneration stem height averaged just over a meter (range 43 to 220 cm), and basal area was low (mean 42 mm^2m^{-2}, range 0-299 mm^2m^{-2}; where 1 mm^2m^{-2} = 0.01 m^2ha^{-1}). On relevé plots, tree regeneration by 13 tree species was quantified, where seven of the more abundant species included two conifers: jack pine and black spruce; five deciduous species: red maple (*Acer rubrum*), paper birch, black ash (*Fraxinus nigra)*, balsam poplar (*Populus balsamifera)*, and quaking aspen. Other measured vegetation included six shrubs, 43 forbs, and seven graminoid species. Vegetation species richness was moderate, averaging 20 species (range 8 to 32). Full descriptive statistics of the plots are provided in Table 5A. Field observations indicated there were substantial spatial pattern differences between aspen and herbaceous cover. Herbaceous vegetation patches were both larger and more evenly distributed compared to patterns observed among the much smaller aspen patches. Aspen stem distributions within relevé plots ranged from a few individuals to multiple, larger patches (2 to 5 m), with substantial variability in arrangements between relevé plots. Nonetheless, patch dimension and arrangement metrics were not explicitly recorded.

In general, the 81 plots were representative of the variability in biophysical attributes for upland regions of the entire PCF (Table 2A and B). Temperature, precipitation, and elevation were most similar between upland areas of the PCF and measured plots. Average plot slope and fire severity were also similar to the average estimated across upland areas of the PCF, but variability was more limited for these variables within measured plots. On average, pre-fire aspen basal area was greater within our 81 field plots compared to that for upland areas across the entire burned

Table 2. Summary of Ecological Data Acquired for (A) Sampled Plot Locations; and (B) Modeled Estimates for the Entire PCF Area. Variables Include Climate (2012), Terrain, Soil Depth to Bedrock (A only), Fire Severity Proxy (Relative Differenced Normalized Burn Ratio, RdNBR), and Aspen Pre-Fire BA. Note that RdNBR is a Relative Measure of Fire Severity (Unitless), where Extreme Values are Generally Greater than 35.

(A)

Ecological Variable	Average	Minimum	Maximum	Std. Dev.
Precip. (mm)	795.35	778.28	816.09	13.56
Temp. (C)	4.79	-15.53	28.09	
Elevation (m)	478.40	455.00	509.00	14.44
Slope (degrees)	2.06	0.00	8.00	1.58
Soil Depth (cm)	34.78	0.00	>150	30.14
Fire Severity	34.89	19.00	41.00	4.28
Pre-fire BA (m^2/ha)	8.73	0.00	36.27	9.62

(B)

Ecological Variable	Average	Minimum	Maximum	Std. Dev.
Precip. (mm)	803.72	770.68	852.11	22.32
Temp. (C)	4.74	-15.95	28.30	
Elevation (m)	487.54	434.00	577.00	22.48
Slope (degree)	2.23	0.00	83.00	4.57
Fire Severity	36.00	1.00	44.00	6.83
Pre-fire BA (m^2/ha)	1.52	0.00	56.00	4.79

area (8.7 versus 1.5 $m^2 ha^{-1}$, respectively), while the range of plot-wise basal areas was less (0-36 versus 0-56 $m^2 ha^{-1}$).

Model Development

Respective cross-validated calibration of post-fire vegetation structure models (Table 3) using field data with remote sensing and biophysical predictor layers resulted in substantially reduced subsets (Table 4) of the original 58 predictors. Retention of the spatially degraded NAIP predictor variables represented a suite of resolutions. For aspen structure, retention of NAIP predictors increased with resolution (i.e., 15, 15, 13, 12, and 9 variables retained at 2-, 5-, 10-, 20-, and 30-m pixel resolution, respectively). For overall vegetation richness, retention of NAIP predictors generally decreased with resolution with the highest variable retention at the 20-m scale (Table 4).

Model calibrations resulted in adjusted coefficients of determination (Adj. R^2) of 0.60 (RMSE = 2.47 species) for vegetative RIC and 0.53 (RMSE = 2.21 mm) for aspen DIA, each with $p < 0.001$. Calibration of the aspen stem DIA model was superior to all other aspen structure models followed by BA, HT, DEN, and PC (Table 3).

Measured response variables and modeled estimates of those variables mapped for upland areas of the PCF (Plate 2), were most similar for aspen DEN, aspen BA and RIC (Table 5A, and B). For all variables except one (PC), the mapped range in variables contained the range observed in the plot data and fell within ecologically plausible bounds.

Relationships between Predictor and Response Variables

Partial least squares regression component loading results for the six cross-validated models of post-fire aspen structure and species richness (Table 3, 4; Figure 3) show DEN as retaining the highest number of predictor variables (32), followed by DIA, RIC, HT, BA, and PC (range 9 to 27). Model coefficient loadings on pre-fire aspen BA and elevation indicate that these variables were the strongest predictors, respectively, for DEN and BA (Figure 3). Elevation (used by all models except RIC) and climate variables (used by all models except PC and DEN) were also strong predictors for DIA, HT, and BA (Figure 3). The PC model had N5 (IR), L8 (GR), and elevation as the strongest predictors, while the RIC model showed strong loading coefficients on both climate and L8 NDVI (16 September 2013).

Model calibrations for DIA, HT, BA, and RIC all retained climate predictor variables (PRECIP and TEMP, Tables 3, 4; Figure 3), which, due to their 4-km resolution, influenced the visual appearance of extrapolated estimates of these structure variables (Plate 2). Because accuracy and detail of information

Table 3. Structure Model Calibration Regression and Leave-One-Out Cross-Validation Results. The Five Dependent Aspen Structure Variables are Stem Density (DEN), Stem Diameter (DIA), Stem Height (HT), Percent Foliar Cover (PC), and Basal Area (BA). The One Dependent Herbaceous Vegetation Structure Variable is Species Richness (RIC).

Dep. Variable	n	R^2	Adj. R^2	RMSE	PRESS	p-value	B_0	B_1	Vars. Initial	Vars. Used	Predictor Images
DEN (stems*m^{-2})	81	0.41	0.40	0.43	0.84	<0.001	0.35	0.41	50	32	N2, N5, N10, N20, N30, L8, ELEV, PF_ASP_BA, SLP
DIA (mm)	81	0.54	0.53	2.21	0.75	<0.001	3.08	0.54	50	27	N2, N5, N10, N20, N30, L8, MIN_TEMP, ELEV, PF_ASP_BA
HT (cm)	81	0.43	0.42	25.55	0.82	<0.001	49.11	0.43	50	13	N2, N10, N20, N30, L8, MIN_TEMP, ELEV
PC (%)	72	0.23	0.22	5.72	0.92	<0.001	6.92	0.23	58	9	N5, N10, N30, L8, W1, ELEV
BA (mm^2*m^{-2})	81	0.46	0.45	33.54	0.77	<0.001	22.69	0.46	50	10	N2, N5, N30, L8, MIN_TEMP, ELEV, PF_ASP_BA
RIC (spp*/0.04 ha^{-1})	81	0.60	0.60	2.47	0.68	<0.001	8.18	0.60	50	16	N5, N10, N20 N30, L8, MEAN_TEMP

Table 4. Predictor Variables Retained by xPLS Regression for Each of the Vegetation Structure Models. Structure Variables are Vegetation Species Richness (RIC) and Aspen Structure Variables: Density (DEN), Diameter (DIA), Height (HT), Percent Cover (PC), and Basal Area (BA).

Dependent Variable	Predictor image variables
DEN (stems*m^{-2})	GR10, RD10, IR10, SR10, NDVI10, BL20, RD20, IR20, SR20, NDVI20, BL2, RD2, IR2, SR2, NDVI2, BL30, RD30, IR30, SR30, NDVI30, RD5, IR5, SR5, NDVI5, LT8_4, LT8_5, SR, SVR, RA, Elevation, Pre-fire aspen BA, Slope
DIA (mm)	BL10, GR10, RD10, SR10, NDVI10, BL20, GR20, RD20, SR20, NDVI20, BL2, GR2, IR2, SR2, NDVI2, GR30, BL5, GR5, RD5, IR5, SR5, NDVI5, MSI, RA, MIN_TEMP, Elevation, Pre-fire aspen BA
HT (cm)	BL10, RD10, RD20, IR20, RD2, SR2, NDVI2, BL30, SR, MSI, RA, MIN_TEMP, Elevation
PC (%)	GR10, RD30, GR5, IR5, LT8_3, SVR, W3, W4, Elevation
BA (mm^2*m^{-2})	RD2, IR2, NDVI30, RD5, SR5, NDVI5, LT8_3, MIN_TEMP, Elevation, Pre-fire aspen BA
RIC (spp*0.04ha^{-1})	SR10, NDVI10, BL20, GR20, RD20, SR20, NDVI20, BL30, GR30, RD30, SR30, BL5, NDVI5, LT8_2, NDVI, MEAN_TEMP

Table 5. Descriptive Statistics for (A) Ground-Measured Vegetation Recovery Data Across All Field Plots, and (B) Modeled Estimates of Aspen Structure and Richness for the Entire PCF. Listed are the five Post-Fire Aspen Regeneration Structure Estimates (Density [DEN], Diameter [DIA], Height [HT], Percent Cover [PC], and Basal Area [BA]) and One Vegetation Species Richness Estimate (RIC).

(A)

Structure Variable	Average	Minimum	Maximum	Std. Dev.
DEN (stems *m^{-2})	0.59	0.00	3.71	0.87
DIA (mm)	8.98	3.41	13.69	2.24
HT (cm)	109.27	42.80	219.85	28.11
PC (%)	8.73	0.00	88.00	13.32
BA (mm^2*m^{-2})	41.60	0.00	299.40	66.92
RIC (spp*0.04ha^{-1})	20.51	8.00	32.00	5.02

(B)

Structure Variable	Average	Minimum	Maximum	Std. Dev.
DEN (stems*m^{-2})	0.66	0.00	3.31	0.49
DIA (mm)	7.12	0.00	26.34	4.95
HT (cm)	94.39	0.00	318.93	54.89
PC (%)	10.75	0.00	42.65	6.38
BA (mm^2*m^{-2})	59.40	0.00	298.33	46.21
RIC (spp*0.04ha^{-1})	21.95	0.75	38.56	3.78

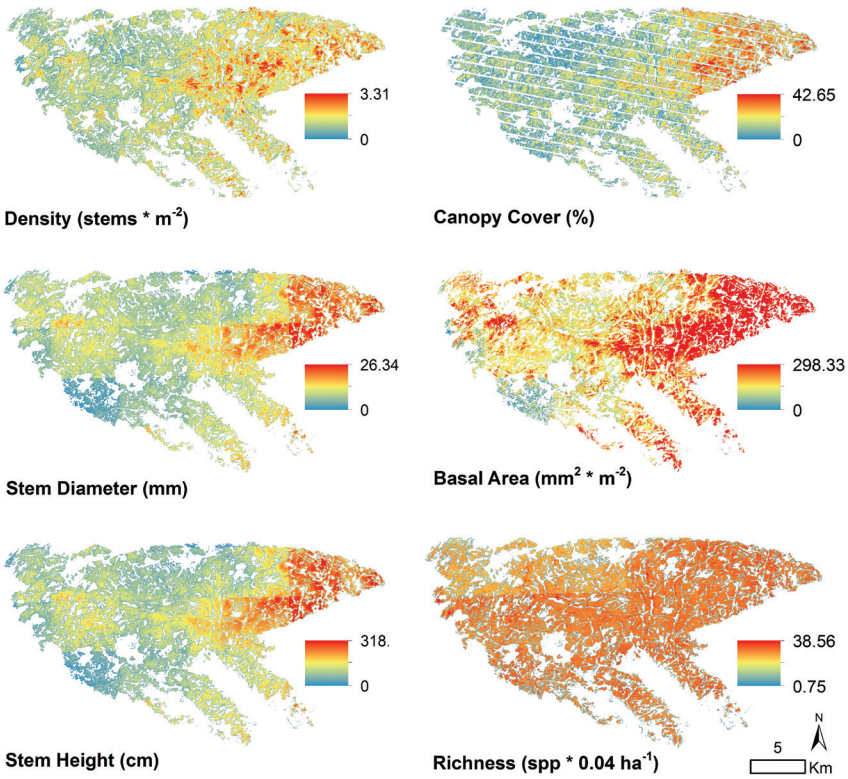

Plate 2. Maps of modeled aspen structural parameters and overall richness. One image used to calibrate the aspen canopy cover model was the winter image (W1, Landsat-7, 23 January 2014); hence, scan line corrector (SLC) failure errors are observed and manifested in these model estimates.

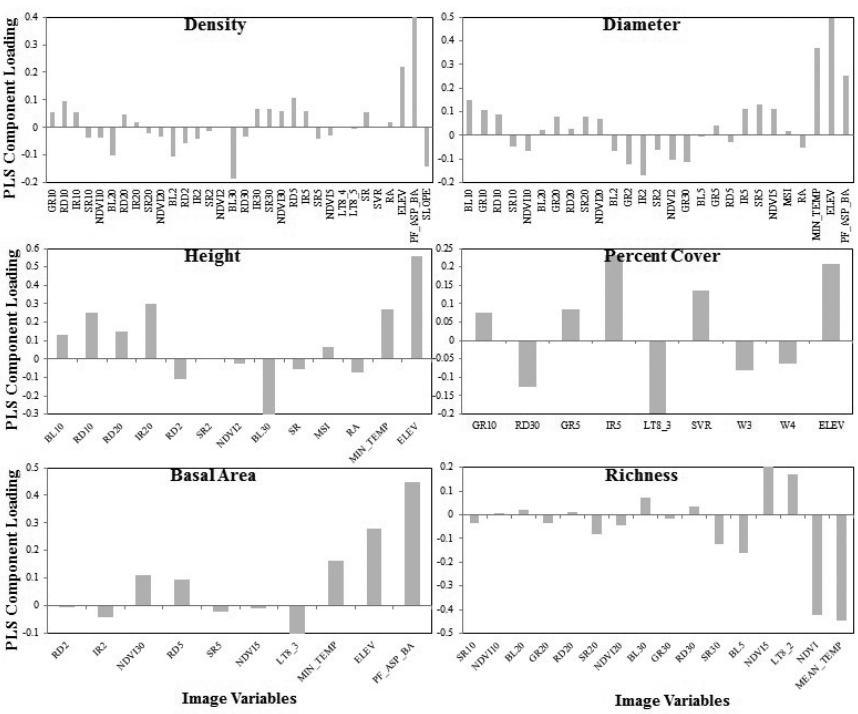

Figure 3. Scaled component loadings for image predictor variables selected by iterative exclusion partial least squares regression (xPLS) during calibration of aspen abundance and vegetation richness models.

decreases as pixel-size increases, we experimented with calibrations that excluded climate variables. This resulted in slight decreases in model fit for DIA (Δ Adj. R^2 = –0.03), HT (Δ Adj. R^2 = –0.01), BA (Δ Adj. R^2 = –0.02), and RIC (Δ Adj. R^2 = –0.05), but a more substantial decrease in model fit for RIC (Δ Adj. R^2 = -0.25). All model calibrations excluding climate predictors remained significant ($p < 0.001$; Table 6A).

Simple linear regression analysis between response variables and pre-burn aspen BA indicated significant ($p < 0.001$) positive relationships in all but two cases (Table 7A). Pre-burn aspen BA was most strongly related to post-burn aspen BA (Adj. R^2 = 0.33), followed by DEN (Adj. R^2 = 0.20), DIA (Adj. R^2 = 0.17), and HT (Adj. R^2 = 0.12), while pre-burn aspen BA did not significantly explain observed variance in PC (p = 0.03, Adj. R^2 = 0.05) or RIC (p = 0.46, Adj. R^2 = -0.01) (Table 7A). By contrast, fire severity (i.e., RdNBR) was not significantly related to any of the response variables (p-value range 0.14 to 0.57, Adj. R^2 range 0.02 to –0.01, Table 7B). These results are consistent with the xPLS results that retained pre-burn aspen BA for corresponding variables (except HT), but did not retain RdNBR for any of the models. Excluding pre-burn BA from the three models that retained this variable did yield significant models ($p < 0.001$; Table 6B). However, for DEN and BA the number of predictors in the final models were substantially reduced (Figure 4), and corresponding model fit was also reduced (DEN: Δ Adj. R^2 = -0.25, BA: Δ Adj. R^2 = -0.25). The model for DIA was far less affected, by excluding pre-burn BA (Δ Adj. R^2 = 0.03).

Discussion

Mapping Early-Seral Forest Composition

This study found that ground and remote sensing data may be used in combination to develop biophysical models of early-seral stage forest vegetation recovery in boreal to sub-boreal forests of the upper Midwestern US. This is particularly important as greater detail is needed to understand forest successional trends in a landscape dominated by fire, and to assist research that strives to forecast future forest composition in lieu of multiple stressors, such as climate change (Soja *et al.*, 2007).

Remote detection of hardwood stand development two to three years following disturbance using medium resolution satellite sensors is thought to be problematic (Coppin and Bauer, 1994), which has limited structural quantification to simple regeneration classes (Wolter and White, 2002) or age categories (Hall *et al.*, 1991). While the use of Landsat time series has improved monitoring of forest recovery stages (Kennedy *et al.*, 2010),

Table 6. Results of Aspen and Vegetation Structure Model Calibrations/Cross-Validations (n = 81) where (A) 4 km climate Predictor Variables, and (B) the Pre-Fire Aspen BA Predictor, Respectively, were Intentionally Withheld During the Iterative Exclusion Partial Least Squares (xPLS) Calibration Procedures.

(A)

Structure Variable	R^2	Adj. R^2	RMSE	PRESS	B_0	B_1	p-value	Vars. Init.	Vars. Used	Predictor Images
DIA (mm)	0.40	0.39	2.21	0.84	3.98	0.40	<0.001	46	23	N2, N5, N10, N20, N30, L8, ELEV, PF_ASP_BA
HT (cm)	0.42	0.41	25.45	0.84	50.22	0.42	<0.001	46	21	N2, N5, N10, N20, N30, L8, ELEV, PF_ASP_BA
BA (mm^2*m^{-2})	0.44	0.43	33.43	0.79	23.35	0.44	<0.001	46	9	N2, N5, N30, L8, ELEV, PF_ASP_BA
RIC ($spp*0.04ha^{-1}$)	0.55	0.55	2.51	0.73	9.16	0.55	<0.001	46	18	N2, N5, N10, N20 N30, L8, ELEV

(B)

Structure Variable	R^2	Adj. R^2	RMSE	PRESS	B_0	B_1	p-value	Vars. Init.	Vars. Used	Predictor Images
DEN ($stems*m^{-1}$)	0.16	0.15	0.32	0.88	0.50	0.16	<0.001	49	6	N10, N20, N30, MAX_TEMP, ELEV
DIA (mm)	0.51	0.51	2.21	0.77	3.25	0.51	<0.001	49	20	N2, N5, N10, N20, L8, MIN_TEMP, ELEV
BA ($mm2*m^{-2}$)	0.21	0.20	27.33	0.88	32.99	0.21	<0.001	49	9	N2, N10, N30, L8, MIN_TEMP, ELEV

Table 7. Plot-Based, Simple Linear Regression Results for Plot-Wise Aspen and Vegetation Dependent Structure Variables (n = 81): Stem Density (DEN), Stem Diameter (DIA), Stem Height (HT), Percent Cover (PC), Basal Area (BA), and Vegetation Species Richness (RIC); Each as a Function of the Independent Predictor (A) Pre-Fire Aspen BA and (B) RdNBR Fire Severity Proxy.

(A)

Plot Variable	R^2	Adj. R^2	p-value	B_0 (95% C.I.)	B_1 (95% C.I.)
DEN ($stems*m^{-2}$)	0.21	0.20	<0.001	5.72 (3.41 - 8.03)	5.08 (2.87 - 7.30)
DIA (mm)	0.18	0.17	<0.001	2.59 (-0.94 - 6.13)	0.92 (0.48 - 1.37)
HT (cm)	0.13	0.12	<0.001	2.82 (-1.11 - 6.74)	0.07 (0.03 - 0.11)
PC (%)	0.06	0.05	0.03	7.18 (4.69 - 9.66)	0.18 (0.02 - 0.34)
BA (mm^2*m^{-2})	0.34	0.33	<0.001	5.35 (3.31 - 7.39)	84.41 (57.87 - 110.96)
RIC ($spp*0.04ha^{-1}$)	0.01	-0.01	0.46	12.01 (2.98 - 21.05)	-0.16 (-0.59 - 0.27)

(B)

Plot Variable	R^2	Adj. R^2	p-value	B_0 (95% C.I.)	B_1 (95% C.I.)
DEN ($stems*m^{-2}$)	0.01	-0.01	0.47	34.65 (33.50 - 35.81)	0.40 (-0.71 - 1.50)
DIA (mm)	0.01	-0.01	0.49	34.38 (32.65 - 36.11)	0.08 (-0.14 - 0.29)
HT (cm)	0.01	0.00	0.30	34.05 (32.19 - 35.92)	0.00 (0.00 - 0.03)
PC (%)	0.02	0.00	0.25	35.25 (34.12 - 36.39)	-0.04 (-0.11 - 0.03)
BA (mm^2*m^{-2})	0.00	-0.01	0.57	34.72 (33.61 - 35.84)	4.12 (-10.35 - 18.60)
RIC ($spp*0.04ha^{-1}$)	0.03	0.02	0.14	32.02 (28.04 - 35.40)	0.14 (-0.05 - 0.33)

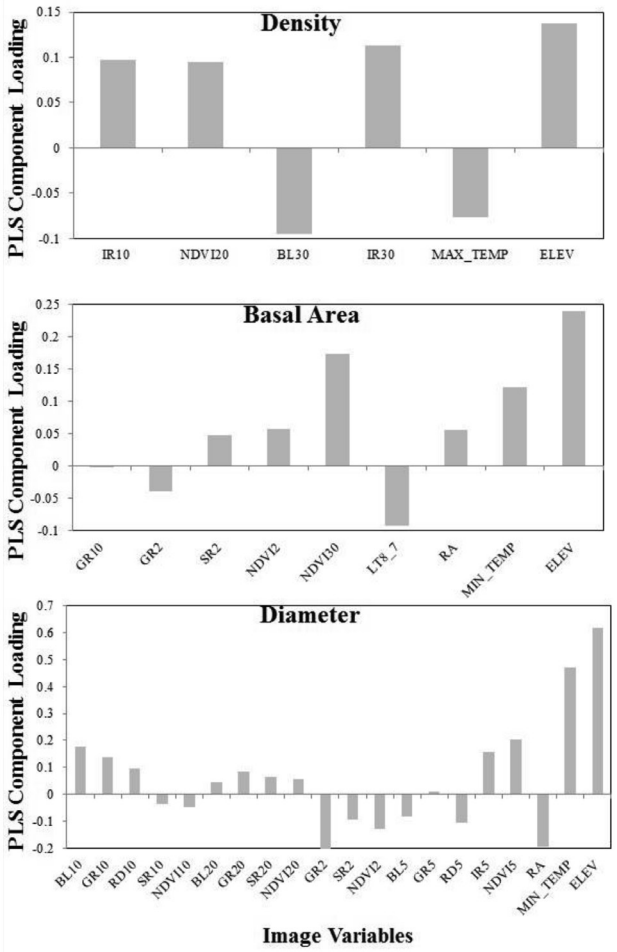

Figure 4. Scaled component loadings for image predictor variables selected by iterative exclusion partial least squares regression (xPLS) during calibration of aspen abundance and vegetation richness models, with pre-fire aspen BA excluded as a predictor variable.

characterization of specific structural variables has lagged behind. Airborne light detection and ranging (lidar) transect data were used recently with Landsat time series data in Canada to model 75th quantile heights and percent canopy cover (above two meters) for regenerating aspen patches in five-year increments up to 25 years following fire disturbance (Bolton *et al.*, 2015), which represented a significant advance over past remote sensing efforts. The cross-validated accuracy results for percent aspen canopy across all age classes was reported as 86.7 percent, while direct measures of aspen density were not reported. While our cross-validated accuracy results for aspen PC (Adj. R^2 = 0.22; RMSE 5.7 percent), HT (Adj. R^2 = 0.42; RMSE 25.5 cm), and other structure estimates (mapped to the pixel-level for a specific stand age (2 year)) are not directly comparable to these results, Bolton *et al.* (2015) did recognize (as we found) that substantial variability among structure estimates was common. Hence, our detection, modeling, and mapping of specific aspen structural attributes two years after wildfire disturbance using optical imaging remote sensing data marks a first in the literature.

While RIC was stronger (Adj. R^2 = 0.60, Table 3) than the aspen structure models, PCF-wide variation among these estimates was relatively low (Plate 2). Most areas across the PCF study area were mapped as having between 15 and 30 species per 0.04 ha, which paralleled field measurements. Past research has shown that vegetation establishment and variability in species richness are influenced by factors associated with distance to living forest following fire (Turner *et al.*, 1998). If variability in species RIC recorded at our northern and southern plots (closer to PCF edges) was substantially different than RIC

observed at central plot locations (Figure 1) this would have been compelling evidence, but this was not the case. Also, given the fact that fire severity was generally high throughout the PCF (RdNBR >35, Plate 1), it seems reasonable that spatial variability in our mapped estimates of RIC were generally low (see Turner *et al.*, 1997; Wang and Kemball, 2005).

Multi-Resolution Approach - What Did We Gain?

The finer spatial resolutions of the NAIP remote sensing data used in this study were instrumental predictors in all of the vegetation models developed. For each model calibration, the xPLS approach retained several resolutions of NAIP variables along with generally fewer Landsat predictor variables. This is compelling evidence for the strength of a multi-resolution approach in such studies. While we specifically quantified six vegetation parameters in this study, such as percent cover, to be used later for model development, we did not specifically quantify vegetation patch sizes or arrangement; although, we did make note of these general characteristics qualitatively across the 81 plots. Herbaceous vegetation patches were generally both larger and more evenly distributed compared to aspen patches. The fact that the automated predictor variable selection process for the aspen structure models generally drew more variables from the two smallest NAIP pixel sizes (2 and 5 meters; 15 variables each) is compelling evidence for the need to include imagery at these spatial resolutions to derive mapped estimates of aspen recovery from remote sensing (Table 4). By contrast, vegetation RIC models, with generally larger observed patch sizes, were weighted more heavily on NAIP predictors of larger pixel sizes (Table 4).

By extension, we expect the newer SPOT-6 and SPOT-7 satellite sensor data (launched in 2012 and 2014, respectively); each with 1.5 m panchromatic channels (450-745 nm), 6 m multispectral channels, and a relatively large swath size (60 km) compared to other high spatial resolution sensors should be more effective for monitoring early aspen recovery in this region. Indeed, fusion of either high resolution SPOT data or hyperspectral sensor data with discrete-return or waveform lidar sensor data are certainly promising such applications (Anderson *et al.*, 2008; Bolton *et al.*, 2015). However, for regional monitoring efforts, the development of methods which take advantage of existing space borne assets will likely be more practical.

Biophyscial Factors Affecting Regeneration Patterns

Prior forest composition commonly influences subsequent, post-fire, forest species composition and abundance (Frelich and Reich, 1995; Heinselman, 1996; Johnson *et al.*, 2003). Post-fire tree seedling recruitment (especially quaking aspen, black spruce, and jack pine) is directly related to pre-fire abundance of the respective tree species (Frelich and Reich, 1995; Heinselman, 1996; Johnson *et al.*, 2003), though specific recovery patterns may be modified by competition with regenerating herbaceous cover (Frey *et al.*, 2003). For the PCF area, pre-burn forest structure and composition data (Wolter and Townsend, 2011) indicated that mature aspen cover was prominent in the central, east, and southern regions prior to the PCF, while mature jack pine and black spruce were more dominant within the western region. This arrangement of pre-burn aspen abundance generally mirrored our modeled post-burn mapped estimates of aspen abundance and structure (Plate 2), which were produced both with and without the pre-burn aspen BA data as a predictive variable. Furthermore, gradients of abundance observed among modeled aspen structure results are consistent with a land use history (i.e., logging) that promoted deciduous species including aspen (Heinselman, 1996). Hence, it seems reasonable to suggest that aspen legacy governs aspen response and recovery following wildfire in this region. However, aspen legacy had no effect on vegetative richness.

By contrast, we found no evidence for a relationship between the Landsat-based fire severity proxy (RdNBR; Miller and Thode, 2007) and vegetation regeneration patterns post burn. It is also important to note that the original formulation of this fire severity index, NBR (Key and Benson, 2005), was not retained by any of the six structure models as an important predictor during the xPLS calibration process (Tables 4 and 6). Available studies indicate conflicting patterns between fire severity and its influence on aspen regeneration (Brown and DeByle, 1987; Perala, 1991; Frelich and Reich, 1995; Fraser *et al.*, 2004). Our results align with studies where ground-based measures of fire severity were unrelated to regeneration success among boreal forest species (Jayen *et al.*, 2006). However there were limitations to our study that may have affected this result. Apart from the northwestern corner of the burn that burned more slowly as a surface fire (Plate 1), the vast majority of the PCF burned as a fast-moving crown fire. It is the combination of fire line intensity and residence time that affect heat penetration beneath the ground surface (Smith *et al.*, 2005) known to impact aspen recovery (Brown and Debyle, 1987). Due to the high speed with which the PCF traversed this landscape (eastern 70 percent of the area burned in five hours), we suspect fire residence times were likely low. Indeed, much of the variability in fire severity estimated by RdNBR is reflective of lowland forests that were comparably less impacted, and these lowlands were excluded from our analysis. It is possible that increasing the number and distribution of field plots across the burned area may have improved aspen and vegetation structure estimation models and provided greater power to assess potential relationships with Landsat-based measures of fire severity.

Notably, burn severity indices derived from Landsat are typically more a function of fire effects on overstory than on ground and soil variables (Lentile *et al.*, 2006). The degree to which RdNBR correlates with these particular fire attributes at a Landsat scale is unclear (Smith *et al.*, 2005; Lentile *et al.*, 2006; Soverel *et al.*, 2010), but the use of relatively low spatial resolution sensors (e.g., Landsat) to characterize the fine-grained indicators of fire effects on soil, such as white-colored ash (Smith *et al.*, 2005), are likely limited. Hence, more research should be conducted using improved and more highly resolved measures of fire severity (Parks *et al.*, 2014), especially those derived using airborne hyperspectral imagery (with superior spatial and spectral resolution) that have been used to produce fire severity indices that better characterize conditions on the forest floor surface following wildfire (Kokaly *et al.*, 2007).

Pre-burn aspen BA, climate (mean and minimum TEMP), and terrain variables (slope and elevation) were all found to be strong, empirical predictors of post-burn vegetation structure (Figure 3). Contrary to expectations, terrain aspect was not found to be an influential predictor for any of our model calibrations. This was surprising since aspect affects soil temperature and moisture levels and, thus, vegetation response dynamics (Frey *et al.*, 2003). With that said, topographic relief across the PCF is relatively gentle and fine-grained, which may not be adequately captured using 30-m DEM information. Hence, using higher spatial resolution aspect information in the future (e.g., lidar-derived) may reveal stronger underlying relationships between vegetation recovery patterns and terrain.

With respect to climate, because of the inordinately high predictive strength of climate variables (MIN_TEMP and MEAN_TEMP) in some of the structure model calibrations, especially DIA and RIC (Figure 3), we suspected pixel size (4 km) effects were skewing calibration results. Indeed, distinct steps among climate data values were observed between northern plots (contained within two climate pixels) and those of the central and southern plots (Figure 1); the results of which were manifest in modeled DIA, HT, BA, and RIC results (Plate 2). Therefore, climate predictor variables were intentionally withheld during the recalibration of these structure models. Climate excluded, significant and viable models were still produced (Table 6A), therefore we posit that spatial integrity gained during model recalibration

(without climate predictors) far outweighs the slight loss in estimation accuracy overall. Because of the positive relationship between temperature and species richness in other boreal ecosystems (Kivinen *et al.*, 2006), future investigations of this nature should explore the use of multitemporal Landsat thermal bands to supply finer-grained proxies of climate predictor variables.

Implications and Directions for Future Study

It is clear that fire regimes throughout North America are changing (Soja *et al.*, 2007; Westerling *et al.*, 2011). Considering the influence of wildfires on carbon stocks (Bond-Lamberty *et al.*, 2007) and the likely shifts in the frequency and magnitude of these forest disturbance events (Flannigan *et al.*, 2000), precise modeling of fire behavior and subsequent forest response is key for understanding and forecasting forest carbon dynamics. And, while adaptive forest management may be applied to mitigate fire behavior and intensity (Pollet and Omi, 2002), we must accept that large, stand-replacing fires will occur, especially in large wilderness areas such as the BWCAW. Because patterns of forest stand structure initiated within a few years after fire are maintained through subsequent decades of stand development (Johnstone *et al.*, 2004), spatially-explicit remote sensing and modeling approaches such as those presented here can provide an earliest possible look at future forest composition and enable continued study of factors that may influence stand development through time. This mapping approach can further compliment more detailed field studies of vegetation dynamics by providing vegetative responses across the full range of environmental conditions, characteristic of large landscapes (Sturtevant *et al.*, 2014). Future research should address vegetation patch characteristics and scale, as well as species-specific associations and communities in terms of competition with forest regeneration (Frey *et al.*, 2003), and how such associations might correspond with certain pre-fire cover types and structure as well as post-fire soil characteristics and fire severities (Kolka *et al.*, 2014).

Acknowledgments

This project was funded by the National Science Foundation (RAPID Collaborative Research Grant 1201484) and the USDA Agriculture & Food Research Initiative (McIntire Stennis project: IOW5348) USFS National Fire Plan. The authors would like to thank Superior National Forest for providing research access to the Boundary Waters Canoe Area Wilderness; Lisa Schulte Moore (Iowa State University, Ames, IA), Jonathan Chipman (Dartmouth, Hanover, NH), Eric Gustafson and John Stanovick (USFS, Newtown Square, PA), and Shawn Fraver (University of Maine, Orono, ME) for reviewing earlier drafts of the manuscript; Jared Niemi and Lendie Follett (Iowa State University, Ames, IA) for statistical consulting; and Louis Hilgemann (VI Dept. of Agriculture, Kingshill, VI), Bert and Johnna Hyde (Ely, MN), and Lawson Gerdes (Minnesota DNR, St. Paul, MN) for field assistance and guidance. We also wish to thank the three blind reviewers, whose comments greatly improved the quality of this manuscript.

References

Anderson, J.E., L.C. Plourde, M.E. Martin, B.H. Braswell, M.L. Smith, R.O. Dubayah, M.A. Hofton, and J.B. Blair, 2008. Integrating waveform LIDAR with hyperspectral imagery for inventory of a northern temperate forest, *Remote Sensing of Environment*, 112(4):1856–1870.

Arzani, H., and G.W. King, 1997. Application of remote sensing (Landsat TM data) for vegetation parameters measurement in western division of NSW, *Proceedings of XVIII IGC 1997*, Winnepeg, Manitoba, Canada.

Bolton, D.K., N.C. Coops, and M.A. Wulder, 2015. Characterizing residual structure and forest recovery following high-severity fire in the western boreal of Canada using Landsat time-series and airborne lidar data, *Remote Sensing of Environment*, 163:48–60.

Bond-Lamberty, B., S.D. Peckham, D.E. Ahl, and S.T. Gower, 2007. Fire as the dominant driver of central Canadian boreal forest carbon balance, *Nature*, 450:89–92.

Brown, J.K., and N.V. Debyle, 1987. Fire damage, mortality, and suckering in aspen, *Canadian Journal of Forest Research*, 17(9):1100–1109.

Carlson, D.J., P.B. Reich, and L.E. Frelich, 2011. Fine-scale heterogeneity in overstory composition contributes to heterogeneity of wildfire severity in southern boreal forest, *Journal of Forest Research*, 16:203–214.

Charbonneau, D., F. Lorenzetti, F. Doyon, and Y. Mauffette, 2012. The influence of stand and landscape characteristics on forest tent caterpillar (*Malacosoma disstria*) defoliation dynamics: The case of the 1999-2002 outbreak in northwestern Quebec, *Canadian Journal of Forest Research*, 42:1827–1836.

Coppin, P.R., and M.E. Bauer, 1994. Processing of multitemporal Landsat TM imagery to optimize extraction of forest cover change features, *IEEE Transactions on Geoscience and Remote Sensing*, 32(4):918–927.

Debyle, N.V., and R.P. Winokur, 1985. *Aspen: Ecology and Management in the Western United States*, USDA Forest Service General Technical Report RM-119, Rocky Mountain Forest and Range Experiment Station, Fort Collins, Colorado.

Flannigan, M.D., B.J. Stocks, and B.M. Wotton. 2000. Climate change and forest fires, *Science of the Total Environment*, 262:221–229.

Franklin, J.F., R.J. Mitchell, and B.J. Palik, 2007. *Natural Disturbance and Stand Development Principles for Ecological Forestry*, General Technical Report NRS-19, Newtown Square, Pennsylvania, U.S. Department of Agriculture, Forest Service, Northern Research Station, 44 p.

Fraser, E., S. Landhausser, and V. Lieffers, 2004. The effect of fire severity and salvage logging traffic on regeneration and early growth of aspen suckers in north-central Alberta, *The Forestry Chronicle*, 80(2):251–256.

Frelich, L.E., and P.B. Reich, 1995. Spatial patterns and succession in a Minnesota southern-boreal forest, *Ecological Monographs*, 65(3):325–346.

Frelich, L.E., 2002. *Forest Dynamics and Disturbance Regimes: Studies from Temperate Evergreen-Deciduous Forests*, Cambridge University Press, Cambridge, UK.

Frey, B.R., V.J.Lieffers, S.M. Landhäusser, P.G. Comeau, and K.J. Greenway, 2003. An analysis of sucker regeneration of trembling aspen, *Canadian Journal of Forest Research*, 33:1169–1179.

Geladi, P., and B.R. Kowalski, 1986. Partial least-squares regression: A tutorial, *Analytica Chimica Acta*, 185:1–17.

Hall, F.G., D.B. Botkin, D.E. Strebel, K.D. Woods, and S.J. Goetz, 1991. Large-scale patterns of forest succession as determined by remote sensing, Ecology, pp. 628–640.

Heinselman, M.L., 1996. *The Boundary Waters Wilderness Ecosystem*, University of Minnesota Press, Minneapolis, Minnesota.

Jayen, K., A. Leduc, and Y. Bergeron, 2006. Effect of fire severity on regeneration success in the boreal forest of northwest Quebec, Canada, *Ecoscience*, 13(2):143–151.

Johnson, E.A., H. Morin, K. Miyanishi, R. Gagnon, and D.F. Greene, 2003. A process approach to understanding disturbance and forest dynamics for sustainable forestry, *Towards Sustainable Management of the Boreal Forest*, Chapter 8 (P.J. Burton, C. Messier, D.W. Smith, and W.L. Adamowicz, editors), NRC Research Press, Ottawa, Ontario, Canada.

Johnstone, J.F., F.S. Chapin, III, J. Foote, S. Kemmett, K. Price, and L. Viereck, 2004. Decadal observations of tree regeneration following fire in boreal forests, *Canadian Journal of Forest Research*, 34(2):267–273.

Johnstone, J.F., F.S. Chapin, T.N. Hollingsworth, M.C. Mack, V. Romanovsky, V. and M. Turetsky, 2010. Fire, climate change, and forest resilience in interior Alaska (selected paper from The Dynamics of Change in Alaska's Boreal Forests: Resilience and Vulnerability in Response to Climate Warming, *Canadian Journal of Forest Research*, 40(7):1302–1312.

Jordan, C.F., 1969. Derivation of leaf area index from quality of light on the forest floor, *Ecology*, 50:663–666.

Keeley, J.E., 2009. Fire intensity, fire severity and burn severity: a brief review and suggested usage, *International Journal of Wildland Fire*, 18:116–126.

Kennedy, R.E., Z. Yang, and W.B. Cohen, 2010. Detecting trends in forest disturbance and recovery using yearly Landsat time series: 1. LandTrendr-Temporal segmentation algorithms. *Remote Sensing of Environment*, 114(12):2897–2910.

Key, C.H., and N.C. Benson, 2005. Landscape assessment: Remote sensing of severity, the normalized burn ratio and ground measure of severity, the composite burn index (D.C.

Lutes, editor), *FIREMON: Fire Effects Monitoring and Inventory System*, General Technical Report, RMRSGTR-164-CD: LA1-LA51, Ogden, Utah, USDA Forest Service, Rocky Mountain Research Station.

Kivinen, S., M. Luoto, M. Kuussaari, and J. Helenius, 2006. Multi-species richness of boreal agricultural landscapes: Effects of climate, biotope, soil and geographical location, *Journal of Biogeography*, 33(5):862–875.

Kokaly, R.F., B.W. Rockwell, S.L. Haire, and T.V.V. King, 2007. Characterization of post-fire surface cover, soils, and burn severity at the Cerro Grande Fire, New Mexico, using hyperspectral and multispectral remote sensing, *Remote Sensing of Environment*, 106:305–325.

Kolka, R., B. Sturtevant, P. Townsend, J. Miesel, P. Wolter, S. Fraver, S., and T. DeSutter, 2014. Post-fire comparisons of forest floor and soil carbon, nitrogen and mercury pools with fire severity indices, *Proceedings of the 12th North American Forest Soils Conference, Soil Science Society of America Journal*, Whitefish, Montana, 16-20 June 2013, 78(1):58–65.

Lentile, L.B., Z.A. Holden, A.M. Smith, M.J. Falkowski, A.T. Hudak, P. Morgan, S.A. Lewis, P.E. Gessler, and N.C. Benson, 2006. Remote sensing techniques to assess active fire characteristics and post-fire effects, *International Journal of Wildland Fire*, 15(3):319–345.

Miller, J.D., and A.E. Thode, 2007. Quantifying fire severity in a heterogeneous landscape with a relative version of the delta Normalized Burn Ration (dNBR), *Remote Sensing of Environment*, 109(1):66–80.

Miller, J.D., E.E. Knapp, C.H. Key, C.N. Skinner, C.J. Isbell, R.M. Creasy, and J.W. Sherlock, 2009. Calibration and validation of the relative differenced Normalized Burn Ratio (RdNBR) to three measures of fire severity in the Sierra Nevada and Klamath Mountains, California, USA, *Remote Sensing of Environment*, 113:645–656.

Minnesota Department of Natural Resources (MN DNR), 2003. *Field Guide to the Native Plant Communities of Minnesota: The Laurentian Mixed Forest Province*, Ecological Land Classification Program, Minnesota County Biological Survey, and Natural Heritage and Nongame Research Program, Minnesota Department of Natural Resources, St. Paul.

Minnesota Department of Natural Resources (MN DNR), 2013. *A Handbook for Collecting Vegetation Plot Data in Minnesota: The Relevé Method*, Second Edition, Minnesota Biological Survey, Minnesota Natural Heritage and Nongame Research Program, and Ecological Land Classification Program, Biological Report 92. Minnesota Department of Natural Resources, St. Paul, Minnesota.

National Climatic Data Center (NCDC) and National Oceanic and Atmospheric Administration (NOAA) Climate Data Online (CDO), 2014. National Environmental Satellite, Data, and Information Service (NESDIS), Annual climatological summary, Ely 25 E, MN US, 1999-2012 average temperature and precipitation, URL: *http://www.ncdc.noaa.gov/*: last date accessed: 29 September 2016).

Parks, S.A., G.K. Dillon, and C. Miller, 2014. A new metric for quantifying burn severity: The relativized burn ratio, *Remote Sensing*, 6(3):1827–1844.

Pastor, J., R.J. Naiman, B. Dewey, and P. McInnes, 1988. Moose, microbes, and the boreal forest, *BioScience*, pp. 770–777.

Perala, D.A., 1991. Renewing decadent aspen stands, *Aspen Management for the 21st Century* (S. Navratil and P.B. Chapman, editors), Symposium Proceedings, 20-21 November 1990, Edmonton, Alberta, Forestry Canada, Northwest Region Alberta Forestry, Lands and Wildlife Poplar Council of Canada, pp. 77–82.

Pollet, J., and P.N. Omi, 2002. Effect of thinning and prescribed burning on crown fire severity in ponderosa pine forests, *International Journal of Wildland Fire*, 11(1):1–10.

PRISM Climate Group, Oregon State University,URL: *http://prism.oregonstate.edu*) last date accessed: 29 September 2016).

Rock, B.N., J.E. Vogelmann, D.L. Williams, A.F. Vogelmann, and T. Hoshizaki, 1986. Remote detection of forest damage, *Bioscience*, 36(7):439–445.

Rouse, J.W., Jr., r.h. Haas, J.A. Schell, and D.W. Deering, 1974. *Monitoring Vegetation Systems in the Great Plains with ERTS*, *Proceedings of the Third ERTS Symposium*, NASA AP-351(1):309–317.

Smith, A.M., M.J. Wooster, N.A. Drake, F.M. Dipotso, M.J. Falkowski, and A.T. Hudak, 2005. Testing the potential of multi-spectral remote sensing for retrospectively estimating fire severity in African Savannahs, *Remote Sensing of Environment*, 97(1):92–115.

Soja, A.J., N.M. Tchebakova, N.H.F. French, M.D. Flannigan, H.H. Shugart, B.J. Stocks, A.I. Sukhinin, E.I. Parfenova, F.S. Chapin, III; and P.W. Stackhouse, Jr., 2007. Climate-induced boreal forest change: Predictions versus current observations, *Global and Planetary Change*, 56:274–296.

Soverel, N.O., D.D.B. Perrakis, and N.C. Coops, 2010. Estimating burn severity from Landsat dNBR and RdNBR indices across western Canada, *Remote Sensing of Environment*, 114(9):1896–1909.

Stephens, S.L., N. Burrows, A. Buyantuyev, R. Gray, R.E. Keane, R. Kubian, S.Liu, F. Seijo, L. Shu, K.G. Tolhurst, and J.W. van Wagtendonk, 2014. Temperate and boreal forest mega-fires: Characteristics and challenges, *Frontiers in Ecology and the Environment*, 12(2):115–122.

Sturtevant, B.R., P. Miranda, P. Wolter, P.M.A. James, M.-J. Fortin, and P.A. Townsend, 2014. Forest recovery patterns in response to divergent disturbance regimes in the Border Lakes region of Minnesota (USA) and Ontario (Canada), *Forest Ecology and Management*, 313:199–211.

Turner, M.G., W.H. Romme, R.H. Gardner, and W.W. Hargrove, 1997. Effects of fire size and pattern on early succession in Yellowstone National Park, *Ecological Monographs*, 67(4): 411–433.

Turner, M.G., W.L. Baker, C.J. Peterson, and R.K. Peet, 1998. Factors influencing succession: Lessons from large, infrequent natural disturbances, *Ecosystems*, 1(6):511–523.

Veraverbeke, S., B. Somers, I. Gitas, T. Katagis, A. Polychronaki, and R. Goossens, 2012. Spectral mixture analysis to assess post-fire vegetation regeneration using Landsat Thematic Mapper imagery: Accounting for soil brightness variation, *International Journal of Applied Earth Observation and Geoinformation*, 14(1):1–11.

Wang, G.G., and K.J. Kemball, 2005. Effects of fire severity on early development of understory vegetation, *Canadian Journal of Forest Research*, 35(2):254–262.

Westerling, A.L., M.G. Turner, E.A.H. Smithwick, W.H. Romme, and M.G. Ryan, 2011. Continued warming could transform Greater Yellowstone fire regimes by mid-21st century, *Proceedings of the National Academy of Sciences*, 108(32):13165–13170.

Wolter, P.T. and M.A. White, 2002. Recent forest cover type transitions and landscape structural changes in northeast Minnesota, USA, *Landscape Ecology*, 17(2):133–155.

Wolter, P.T., P.A. Townsend, B.R. Sturtevant, and C.C. Kingdon, 2008. Remote sensing of the distribution and abundance of host species for spruce budworm in northern Minnesota and Ontario, *Remote Sensing of Environment*, 112:3971–3982.

Wolter, P.T., P.A. Townsend, B.R. Sturtevant, 2009. Estimation of forest structural parameters using 5 and 10 meter SPOT-5 satellite data, *Remote Sensing of Environment*, 113:2019–2036.

Wolter, P.T. and P.A. Townsend, 2011. Multi-sensor data fusion for estimating forest species composition and abundance in northern Minnesota, *Remote Sensing of Environment*, 115:671–691.

Wolter, P.T., E.A. Berkley, S.D. Peckham, A. Singh, and P.A. Townsend, 2012. Exploiting tree shadows on snow for estimating forest BA using Landsat data, *Remote Sensing of Environment*, 121: 69–79.

(Received 07 February 2016; accepted 09 May 2016; final version 01 August 2016)